



Experimental study of two-phase flow regimes in slit microchannels

F. V. Ronshin^{1,2} · Yu. A. Dementyev^{1,2} · E. A. Chinnov^{1,2}

Received: 19 September 2022 / Accepted: 8 February 2023 / Published online: 15 March 2023
© The Author(s), under exclusive licence to Springer-Verlag GmbH Germany, part of Springer Nature 2023

Abstract

A two-phase flow in flat minichannels and microchannels with a height range of 50–1 mm and width range of 10–40 mm was experimentally investigated. The flow regimes were determined and regime maps were constructed. The characteristics of two-phase flows have been studied using laser-induced fluorescence and Schlieren methods. Transitions between two-phase flows and their formation have been investigated. Based on the developed methodology, criteria that accurately determine the boundaries between the two-phase flow regimes have been created. The two-phase flow regimes in microchannels were compared with theoretical models. For the Taitel and Dukler and Ullmann and Brauner models, an algorithm that calculates the regime maps for the given channel parameters was derived. It was shown that the Ullmann and Brauner model predicts quite well the transition to the stratified and annular regimes in channels with cross-sections of $0.05 \times 20 \text{ mm}^2$ and $0.05 \times 40 \text{ mm}^2$. Regularities of the channel width influence on the transition to the annular regime were revealed. A criterion for the transition from the stratified to the annular regime, based on the discovered fact of liquid jet structuring along the channel, has been proposed.

Keywords Two-phase flow · Flow regimes · Slit microchannel · Schlieren method · LIF method

1 Introduction

Currently, there is a rapid development of microsystems that are used in microreactors, micropumps, heat exchangers, cooling systems, etc. (Yao et al. 2021; Li et al. 2021). In such systems, the characteristic dimensions of the heat-generating devices are from tens to hundreds of microns. Such systems are more efficient than conventional heat exchangers due to the large area-to-volume ratio. In this regard, micro heat-exchanging devices are widely used. Using microchannel systems, it is possible to remove heat fluxes of more than 1 kW/cm^2 using microchannel systems (Nasr et al. 2017). Two-phase liquid–gas and/or liquid–vapor flows in microchannels have a huge potential to resolve the problem of high heat fluxes removal (Zaitsev et al. 2017). Due to the increased microscale segregation of vapor from the liquid

phase caused by capillary forces as compared to macroscale flows, the flow regimes in microchannels take a more simplified form (Magnini and Thome 2017).

In recent years, interest in the topic of two-phase and two-component flows in microchannels continues to grow due to increased relevance and a large number of unsolved problems. Iqbal and Pandey (2018) have developed a new model for predicting the pressure drop during boiling in a microchannel, since the previous models did not take into account a change in thermophysical properties at large pressure drops. Soma and Kunugi (2020) have developed a phenomenological model for liquid film evaporation in a narrow microchannel. In this work, local heat and mass transfer in the region of a microscopic liquid film is described taking into account thermal conductivity in the liquid film, kinetics, and diffusion. Der and Bertola (2020) have studied a two-component water–oil flow in a horizontal serpentine channel. The regime maps were created and it was shown that the serpentine geometry of the channel reduces the area of stratified flow of two fluids on the regime map, while increasing the areas of intermittent and dispersed flows, which leads to better mixing of two components as compared to the straight channel. In Drummond et al. (2020), the authors investigated the morphology in a single microchannel heat

✉ F. V. Ronshin
f.ronshin@gmail.com

¹ Kutateladze Institute of Thermophysics, Siberian Branch, Russian Academy of Sciences, Lavrentyev ave. 1, Novosibirsk 630090, Russia

² Novosibirsk State University, Pirogov St. 1, Novosibirsk 630090, Russia

sink. Microchannel samples were selected with a high aspect ratio. It was shown that for the channels (1 mm) at sufficiently high heat fluxes, vapor covers the channel base completely, and the liquid did not wet the surface in this area. This newly discovered vaporization phenomenon causes a significant decrease in productivity and an increase in measured channel wall temperatures. This paper demonstrates the critical role of two-phase flow morphology in the operation and design of manifold microchannel heat sinks. Oudah et al. (2020) studied boiling in a microchannel radiator using inlet restrictors. Experiments using inlet restrictors improved the performance of the critical heat flux in a microchannel radiator with a fluidized bed as compared to the basic case without inlet restrictors. The improvements relate mainly to the suppression of flow instability by inlet restrictors. Xiong et al. (2022) have done a comprehensive review of the distribution of two-phase flow in microchannel heat exchangers.

Thus, today in the field of two-phase and two-component flows in small-sized channels, there are many interesting effects and topical problems for various technical applications, in particular, for the design of cooling systems. For more efficient heat removal, it is necessary to understand the hydrodynamics of adiabatic flows in microchannels, in particular, the regimes of gas–liquid flows and criteria for transitions between them since adiabatic regimes often repeat the morphology of heat-exchange liquid–vapor flows with the same void fractions.

Over the past two decades, there were a large number of publications on adiabatic two-phase flows in channels of different geometries, including rectangular channels with characteristic dimensions from 50 μm to 1 mm, square and circular channels with characteristic dimensions of up to 20 μm (Serizawa et al. 2002). Many authors studied microchannels with a circular cross-section (Serizawa et al. 2002; Kawahara et al. 2002; Chung and Kawadji 2004; Chung et al. 2004; Saisorn and Wongwises 2009; Sur and Liu 2011 and others). Also, many authors studied two-phase flow characteristics in square and rectangular channels with a low aspect ratio (Choi and Kim 2010; Yin et al. 2018; Li et al. 2022). The papers on two-phase flow regimes in channels of various geometries and sizes were reviewed by Chinnov et al. (2015). The main factors affecting the structure of a two-phase flow, such as gas and liquid flow rates, channel and inlet parameters, wettability of the inner surface of channels, liquid properties, and gravitational forces have been analyzed. It is shown that the development of instabilities of a two-phase flow has a significant effect on formation, evolution, and transition in the flow regimes. It is necessary to note that the number of works devoted to rectangular channels with a high aspect ratio (slit channels) is very limited. Moriyama et al. (1993) were the first authors who began to study such channels. They studied adiabatic two-phase flows of R113-N2 in channels with a height of 7–98 μm and a

width of 30 mm. This paper deals mainly with the two-phase pressure drop; however, reliability of the results and determination of the channel height are questionable. Most of the works mentioned above used a simple visualization technique of high-speed video recording, which did not allow quantitative determination of two-phase flow characteristics.

The two-phase flow in a short horizontal channel of a rectangular cross-section with a height of 100–500 μm and a width of 9–40 mm was studied experimentally by Chinnov et al. (2016). The use of the Schlieren and fluorescent methods allowed the authors to identify the liquid flow regime in the channel and quantify its characteristics. The features of the churn, jet, and drop flow patterns were studied in detail. Two particular regimes that can be distinguished represent the formation of immobile drops on the channel walls because of the breakage of liquid films or liquid bridges and the appearance of mobile drops due to the two-phase flow instabilities. It was found that the formation of various two-phase flow patterns and transitions between them is determined by instabilities of the liquid–gas flow in the side parts of a channel. Frontal instability has been observed during the liquid–gas interaction in the region of liquid output from the nozzle. It was shown that a change in the height and width of the horizontal channels has a substantial effect on the boundaries between the flow regimes. One of the results is that the region of the churn regime increases significantly with decreasing thickness of the channel.

When designing cooling systems, it is important to determine the gas–liquid flow regime (Wu et al. 2017). In most experimental works, the boundaries between the regimes are determined qualitatively, which reduces the accuracy of their determination. For more than half a century, models predicting the boundaries between flow regimes have been developed. The first attempts to generalize the regime maps of two-phase flows were made by Baker (1954), who proposed an empirical regime map. Since then, there were numerous attempts to predict regime maps, in particular (Mandhane et al. 1974; Taitel and Dukler 1976; Weisman et al. 1979). The most interesting of them is the work of Taitel and Dukler (1976). Their model is used to construct regime maps, where the superficial velocities of gas and liquid are used as coordinates. The model describes four predominant flow regimes: stratified, intermittent, bubble, and annular. Transitions from one regime to another are substantiated using physical criteria. In 1990, after the significant contribution of Barnea et al. (1980); Shoham (1982); Taitel and Dukler (1987), this work culminated in the creation of a unified model for calculating the transitions between flow regimes in channels of any orientation, based on simple physical criteria and using the familiar two-phase dimensionless numbers (Taitel 1990).

Models based on physical criteria used in the regime maps of Taitel and Dukler determine most accurately the

prevailing flow patterns for evaporation of refrigerants and dielectric fluids in channels. Such models can be also used for known macroscale correlations for these dielectric fluids in microchannel cooling systems. Bar-Cohen and Rahim (2009) found that calculations by the Taitel and Dukler model were in good agreement with extensive two-phase flow observational data taken from published sources, and observed inflection points in the behavior of the heat transfer coefficient of a two-phase flow often occur near flow boundaries calculated by Taitel and Dukler. Later, in the work of Bar-Cohen et al. (2011), the authors provided a comprehensive literature review and analysis of microchannel (microgap) heat transfer data for the two-phase flow of refrigerants and dielectric liquids. They showed that flow regime progression in such a microgap channel could be predicted by the traditional flow regime maps, including the regime boundaries, based on Taitel and Dukler model. Data covered the channels with rectangular and slit geometry. Characteristic dimensions of these channels varied from 0.2 to 1.6 mm.

Dimensionless maps ensure a compact way to indicate specific transitions for easier interpretation and more physical representation of flow pattern distribution on a map. However, it is more convenient to use not the dimensionless form of the Taitel–Dukler regime map (Taitel and Barnea 2016), but the maps using the superficial velocities of gas and liquid as the coordinates.

There are a huge number of parameters affecting the structure of a two-phase flow. Until now, no model would accurately predict the regime map for the entire range of used channels. It is necessary to investigate the applicability of models used in the literature for slit microchannels and to develop a model describing the transition to film flow regimes, that is important for practical applications.

Thus, in this introduction, three main problems of investigating two-phase flows in microchannels can be distinguished:

1. Measurement techniques in most studies are based on simple visualization of the two-phase flow (video recording). As a result, it is impossible to obtain quantitative information for the determination of regime boundaries.
2. In most works, qualitative criteria are used to determine the boundaries between two-phase flow regimes in channels, and this reduces the accuracy of determining these boundaries.
3. Models describing regime boundaries, constructed for large circular channels, are often used, successfully, to describe the flow regimes in small rectangular channels. These models cannot be universal, but the limit of their use (in terms of channel width and height) is not defined.

The objectives of this study are as follows:

- to conduct a comprehensive study of a two-phase flow in small horizontal slit channels using modern experimental techniques,
- to analyze data obtained in channels with a height range of 50 μm to 1 mm,
- to clarify the boundaries between the regimes based on quantitative characteristics,
- to create regime maps with more accurate boundaries,
- to perform the comparison of the obtained models with the known ones,
- to determine the applicability limits of these models,
- to provide recommendations for determining the boundaries between the regimes in slit microchannels.

2 Experimental setup and measurement technique

The experiments were carried out in two working sections:

In the first section, experiments were carried out in microchannels with a height from 100 μm to 1 mm. The working section 135 mm long and 60 mm wide was made of stainless steel mounted on textolite, Fig. 1. Flat spacers were aligned in the flow direction so that a channel of variable height and width can be created. The channel width was varied from 9 to 40 mm. The length of the channel was 80 mm. The working section was covered with glass from above. The setup included a liquid circulation circuit, controlled by a computer. Gas was fed from a cylinder through flow meters into a channel, and then it was separated from the liquid and discharged into the atmosphere. The gas was saturated with water vapors before entering the working section. The liquid was supplied with a high-precision peristaltic pump through a flat nozzle into the studied channel. The nozzle was located in a stainless steel plate at the bottom of the working section.

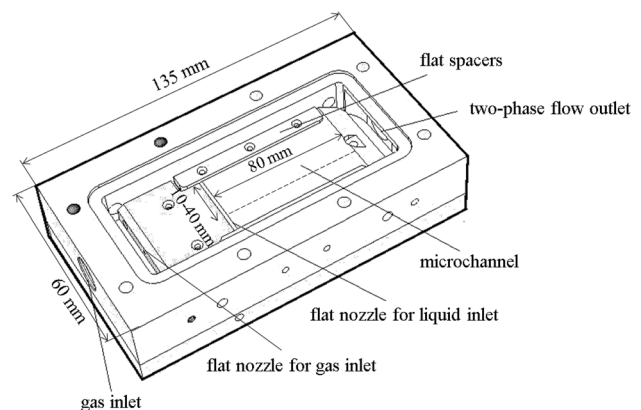


Fig. 1 Working section 1

Gas was supplied to the central part of the channel through the inlet, located at a distance of 40 mm from the liquid input, where the gas flow was stabilized.

For channels less than 100 μm in height, another working section was developed. The outline of working Sect. 2 is shown in Fig. 2. It consists of two parallel plates 160 mm long and 55 mm wide (glass top, stainless steel bottom), the distance between which is set by two constantan spacers with a thickness from 50 to 150 μm . A nozzle is made in the bottom plate at an angle of 11° ; through this nozzle, the liquid is fed to the space between the plates using a high-precision syringe pump. Microchannel dimensions: length of 160 mm, width from 10 to 40 mm, and height from 50 to 150 μm . The wettability and roughness of the channel walls were measured. Wettability was measured by a KRUSS DSA 100 setup using the sessile drop method. On the upper plate (glass with antireflection coating), the advancing contact angle was $63 \pm 1^\circ$, and the receding contact angle was $28 \pm 1^\circ$. On the stainless steel plate, the advancing contact angle was $90 \pm 1^\circ$, and the receding contact angle was $16 \pm 2^\circ$. Surface roughness was measured using a TR200 instrument (resolution 0.001 μm). The roughness of the stainless steel plate was $R_a = 0.47 \mu\text{m}$. The roughness of the upper channel wall of the quartz glass was $R_a = 1 \text{ nm}$. Before the experiment, the liquid was circulating in the microchannel, wetting all the walls. Thus, during the formation of the flow regime, the contact angle was close to the receding one.

The setup is shown in Fig. 3. To visualize the two-phase flow, a FASTCAM-500M high-speed camera and a Nikon D7000 digital camera were used in the mode of Schlieren photography. The Schlieren method is used to register and visualize surface deformations of a thin liquid film. Light from the source enters the microchannel with a gas–liquid flow through a diffuser (7), a lens (8), a semitransparent mirror (9), and an optical glass (10). Light reflected from the gas–liquid interface is transmitted through a semitransparent mirror (9), a lens (11), and a camera lens filter (12). A sheet (13) moved by a microscrew cuts out the central part of the light. As a result,

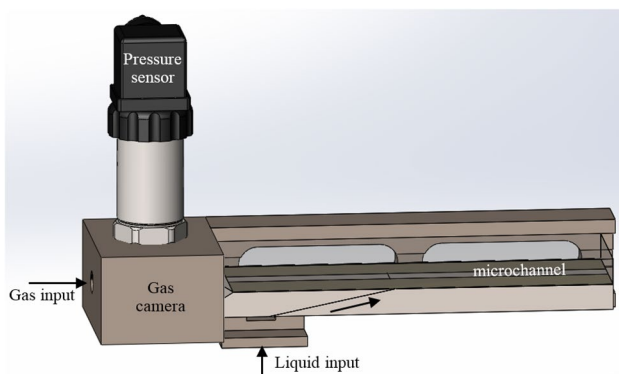


Fig. 2 Working section 2

the camera captures the image in grayscale, where a certain angle of liquid–gas interface inclination corresponds to each level of gray. A detailed description of the methodology and calibration is presented by Ron'shin et al. (2016). Further, the images are processed using the developed algorithm to obtain quantitative characteristics of two-phase flow regimes. A detailed description of the technique is presented by Ronshin and Chinnov (2019).

The method of laser-induced fluorescence is based on absorbed light re-emission by fluorophore with a spectral composition different from exciting radiation. Distilled water with the addition of fluorophore Rhodamine 6G was used as a liquid, and nitrogen or air was used as gas. To excite reference radiation, a 50 mW laser (14) with a wavelength of 532 nm was used. Using a cylindrical lens (15), the laser beam was turned into a line, directed across the gas–liquid flow at a distance of 52 mm from the place where liquid was introduced into the channel. The re-emitted fluorescent light was fixed by a digital camera (17) equipped with a stepped low-frequency filter (16), which transmitted the light re-emitted by a fluorophore and cut off laser radiation. The camera allows for digitizing the received signal, used to determine the distribution of liquid in the channel, with a high sampling rate (up to 2.1 kHz). The measuring system was calibrated under the experimental conditions by the local glow intensity of plane-parallel layers of the working liquid in a completely filled channel. The LIF method allows registration structures in the flow with good accuracy (uncertainty $<3\%$) with good spatial (80 $\mu\text{m}/\text{pix}$) and temporal resolutions (2 kHz) when the thickness of the liquid layer changes significantly. However, it does not allow resolving structures on liquid films with good accuracy. The fluorescence method was used for channels with a height of 200 μm to 1 mm because, in smaller channels, its accuracy is insufficient to characterize the flow regime. In channels less than 200 μm in height, the accuracy of the LIF method decreases and is insufficient to determine accurately the characteristics of the two-phase flow. Calibration of the method is also a difficult task since the typical film thicknesses can be less than 1 μm . Only the Schlieren method, which can detect liquid films less than 1 μm thick, was used in channels with a height of 50 μm –150 μm .

3 Flow regimes

The two-phase flow in short horizontal rectangular channels with a height from 1 mm to 50 μm was experimentally investigated (the list of channels studied is given in Table 1). Instant Schlieren and LIF images of two-phase flow patterns were obtained in the initial part of the channel at a distance of up to 40 mm from the liquid input. Based on Schlieren images, thin liquid films on the channel walls were registered. In this modified Schlieren

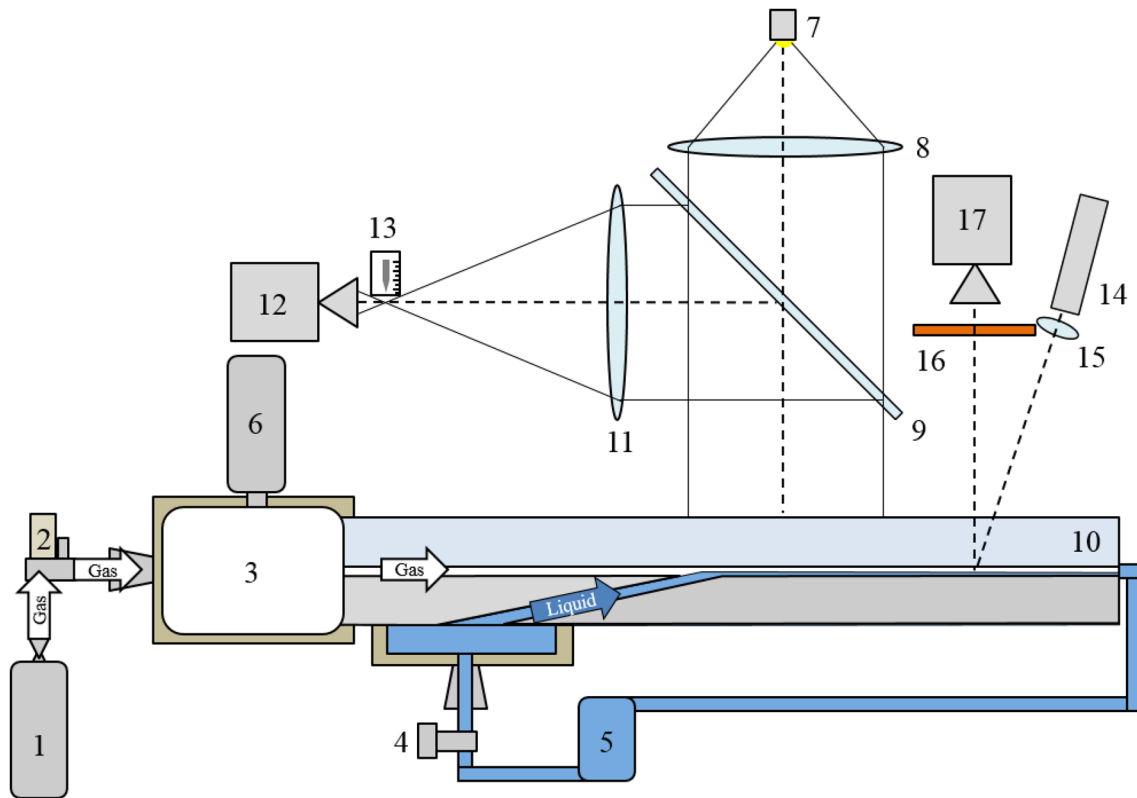


Fig. 3 Scheme of the experimental setup

method, each shade corresponds to a value (dry area, film on the upper microchannel wall, film on the lower microchannel wall, liquid-filled area). Post-processing of the obtained images allowed accurate fixing of the two-phase flow structure in the channels. Based on the information obtained during the post-processing of images, as well as from the analysis of video records, LIF and Schlieren visualization, the main regimes of a two-phase flow were determined and regime maps of the flow process were constructed for various channels.

The regime map for a channel with a cross-section of $0.05 \times 20 \text{ mm}^2$ is shown in Fig. 4. Typical Schlieren photographs are shown for the main two-phase flow regimes. We used

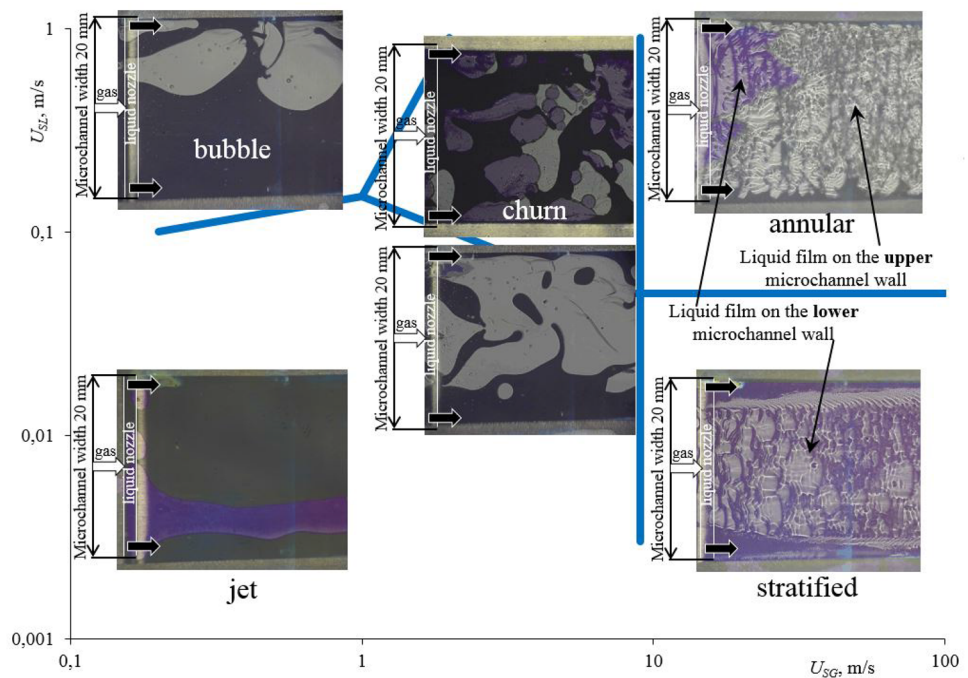
the superficial velocities of gas U_{SG} and liquid U_{SL} , defined as the volumetric flow rate of gas or liquid divided by the channel cross-sectional area, as the coordinates in the figure. The boundaries of the flow regimes for a channel with a cross-section of $0.05 \times 20 \text{ mm}^2$ are indicated by solid lines. The following flow regimes have been identified: bubble, jet, stratified, churn, and annular.

At low superficial velocities of gas and liquid, a stratified flow is observed, when liquid moves along the side walls of the channel, and the gas jet moves along the center. Waves are observed along the side walls. With an increase in the superficial velocity of the liquid, the wetted region increases, the waves of liquid along the side walls begin to interact,

Table 1 Channel dimensions and methods of investigation

Channel cross-sections, mm^2				Working section	Investigation method
1	2	3	4		
0.05 × 10	0.05 × 20	–	0.05 × 40	2	Schlieren
	0.1 × 20	0.1 × 30	–	2	Schlieren
0.15 × 10	0.15 × 20	–	–	2	Schlieren
–	–	0.2 × 34	–	1	Schlieren, LIF
0.3 × 10	0.3 × 20	0.3 × 30	0.3 × 40	1	Schlieren
0.42 × 9	0.49 × 20	0.44 × 30	–	1	LIF, Video recording
1 × 10	1 × 19	1 × 29	1 × 40	1	LIF, Schlieren, Video recording

Fig. 4 Regime map of the two-phase flow in the channel with cross-section of $0.05 \times 20 \text{ mm}^2$



forming horizontal liquid bridges, and a transition to the bubble flow occurs. In the bubble flow regime, many small gas bubbles move along the channel, while the characteristic longitudinal dimensions of bubbles are less than the channel width. The frequency of bubble formation depends significantly on the superficial velocities of gas and liquid. A more detailed study of the frequency of bubble formation and their sizes is presented in Ronshin and Chinnov (2019). With an increase in the superficial velocity of the gas, the size of bubbles increases and coalescence begins. A churn flow regime develops when both filled and destroyed horizontal liquid bridges are observed in the flow. This regime is typical of the vertical channels, but it is also observed in the horizontal minichannels and microchannels, where its formation is caused by capillary forces. At low superficial velocities of liquid and high superficial velocities of gas, a stratified regime is observed, when a liquid film moves along the lower wall of the channel, entrained by the gas flow. The formation of waves is observed on the liquid film surface. With an increase in the superficial velocity of the liquid, a film is also formed on the upper wall, and a transition to the annular flow occurs. In this flow regime, liquid films move along all channel walls, and a gas core with liquid droplets moves along the channel center. Quantitative criteria for transitions between flow regimes are presented by Ronshin et al. (2019). The developed modified Schlieren method allows us to obtain information about the structure of a flat flow, such as the size and velocity of bubbles, film regions on the upper and lower walls of the channel, local void fraction, etc. This information is sufficient for determining the transitions between flow regimes. However, it is not

possible to obtain information on the three-dimensional flow pattern using the Schlieren method.

Figure 5 shows the regime map for a microchannel with a height of $440 \mu\text{m}$ and a width of 30 mm . The LIF method is well suited for characterizing the three-dimensional flow. In addition to the already considered flow regimes, which were observed in a microchannel with a height of $50 \mu\text{m}$, the slug flow regime is also distinguished, when bubbles, whose longitudinal size exceeds the microchannel width, move along this microchannel.

The time dependences of liquid distribution in the channel cross-section were obtained using the fluorescence method. Figure 6 shows three-dimensional flow patterns, reconstructed from the brightness of fluorophore luminescence,

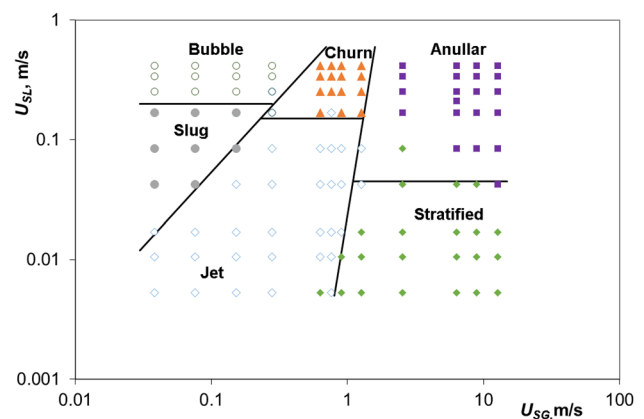


Fig. 5 Regime map of the two-phase flow in the channel with cross-section of $0.44 \times 30 \text{ mm}^2$

characteristic of different flow regimes over time. The time scales are shown in the images. The width of the image corresponds to the width of the channel. Figure 6a shows the typical bubble flow at $U_{SL}=0.42$ m/s, $U_{SG}=0.28$ m/s. Gas bubbles, whose longitudinal size does not exceed the microchannel width, move along this microchannel. As the superficial gas velocity increases, the bubble formation frequency increases. In the transition to the churn flow with an increase in the superficial gas velocity, the bubbles coalesce, due to which the frequency of their formation decreases.

Figure 6b shows the churn flow regime at $U_{SL}=0.42$ m/s, $U_{SG}=1.3$ m/s. Bubble coalescence is characterized by the appearance of ruptures in the horizontal liquid bridges; thus, the churn flow is characterized by the presence of both continuous and broken horizontal liquid bridges. At low superficial velocities of liquid, a jet flow regime is observed, when a gas jet moves along the channel center and liquid moves along the side walls of the channel. In a jet flow, an increase in the superficial liquid velocity leads to a loss of stability of the two-phase flow. Increasing pulsations of the gas jet are

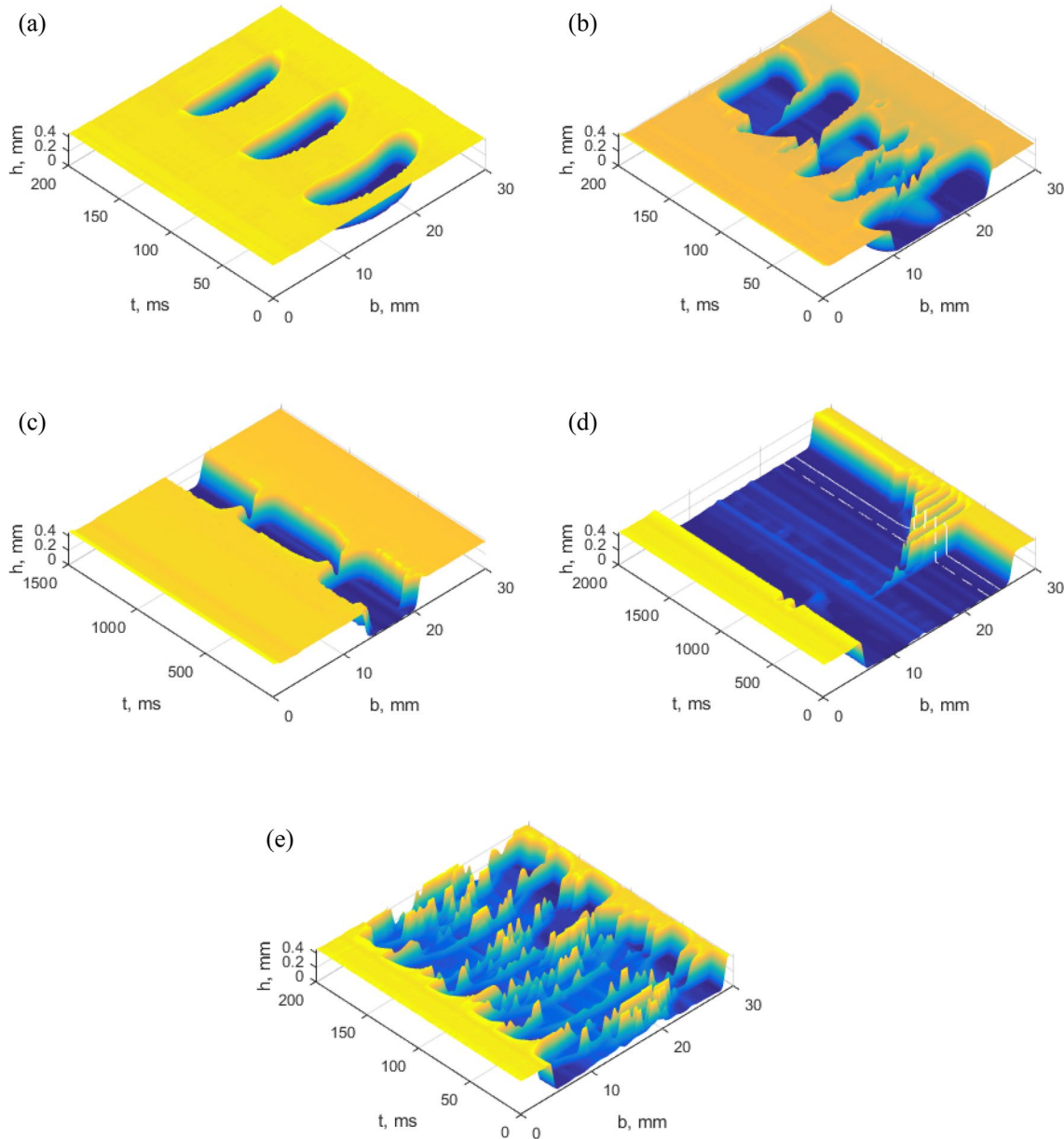


Fig. 6 Flow regimes in a horizontal channel with a width of 30 mm, a length of 80 mm, and a height of 0.44 mm: (a) bubble flow regime at $U_{SL}=0.42$ m/s, $U_{SG}=0.28$ m/s; (b) churn flow regime at $U_{SL}=0.42$ m/s, $U_{SG}=1.3$ m/s; (c) jet flow regime at $U_{SL}=0.17$ m/s,

$U_{SG}=0.76$ m/s; (d) stratified flow regime at $U_{SL}=0.042$ m/s, $U_{SG}=6.4$ m/s; (e) annular flow regime at $U_{SL}=0.17$ m/s, $U_{SG}=8.9$ m/s

observed. At the initial stage of disturbance development, after a long waiting period from 5 to 10 s, the jet collapsed (the liquid was connected from the sides of the channel), Fig. 6c. Then the jet expanded sharply, with a period of 0.4 s, and narrowed several times until the oscillations were completely damped. In the area of stratified flow, the first disturbances also occurred after a significant waiting period.

Figure 6d shows the reconstructed change in the thickness of liquid h in the channel over time based on the reduced change in the fluorophore brightness for a stratified flow at $U_{SL}=0.042$ m/s, $U_{SG}=6.4$ m/s. Before the onset of the disturbance, the liquid layer increased on one of the lateral sides of the channel. The average development time of disturbance is 0.7 s, the waiting time is 5.3 s, and the period between decaying liquid ejections is 91 ms. On the opposite side of the channel, changes, associated apparently with the development of a disturbance, appeared at the boundary of the liquid completely filling the channel. The maximum disturbance amplitude was 11.7 mm and it almost reached the middle of the channel. Figure 7 shows the changes in the liquid height over time along the lines shown in Fig. 6d. It can be seen that for the section (indicated by a solid line) located closer to the lateral side of the channel (distance from the left wall $X=5$ mm), the passing disturbances completely fill the channel height of 0.44 mm. In the region where the phase boundary passes, the reconstructed values of liquid thickness can exceed the channel thickness, which is caused by optical distortions. The magnitude of the possible error in determining the liquid layer thickness does not exceed 40 μm , which is less than 10% of the channel thickness. In the section (indicated by a solid line located at a distance of 6.4 mm from the left channel wall, Fig. 7), not four, but three disturbances were recorded. After the passage of disturbances, an increase in the residual thickness of the liquid film is seen. It follows from the video recording of the process that a thin liquid film appears on the upper wall of the channel because of disturbance passage. With an increase in the superficial liquid velocity, the stratified flow regime

is transformed into an annular one due to an increase in the frequency of pulsations and ejection of liquid onto the upper wall from the side walls of the channel. Figure 6e shows the average thickness of the liquid film on the upper and bottom microchannel walls in the annular regime at $U_{SL}=0.17$ m/s, $U_{SG}=8.9$ m/s. The annular regime at the measurement point occurs at a liquid pulsation frequency in the lateral part of the channel of 20–30 Hz, and the maximum values of pulsation frequency in the annular regime in the investigated parameter range reach 300–400 Hz.

4 Comparison of experimental data with Taitel and Dukler model

An algorithm in MATLAB[®] that calculates the main regimes of two-phase flow according to the Taitel and Dukler model (Taitel 1990) for the specified properties of liquid, gas, and channel size, has been derived. The program works as follows: during the cycle, the superficial velocities of gas and liquid change in a given range. Equations 1–4, obtained from the balance of liquid and gas momentum, are used to find the equilibrium level of liquid (h_L/D) for a steady stratified flow when pressure gradients of liquid and gas are equal to each other. Since the value of function h_L/D is given implicitly in these equations, they were solved by the Newton–Raphson method (Fig. 8).

$$-\frac{\tau_L S_L}{A_L} + \frac{\tau_G S_G}{A_G} + \tau_i S_i \left(\frac{1}{A_L} + \frac{1}{A_G} \right) - (\rho_L - \rho_G)g \sin \beta = 0, \tag{1}$$

where shear stress is expressed in terms of friction factors f_L, f_G :

$$\tau_L = f_L \frac{\rho_L U_L^2}{2} \tag{2}$$

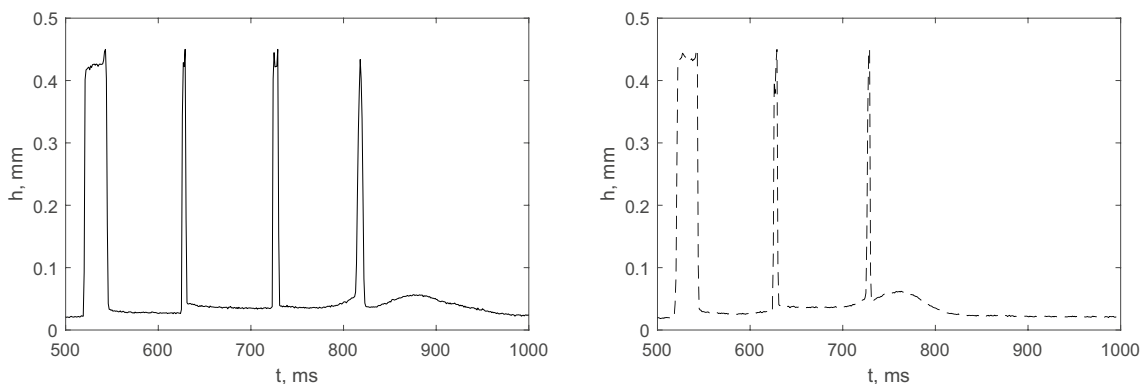


Fig. 7 The liquid thickness distribution in the section shown in Fig. 6d

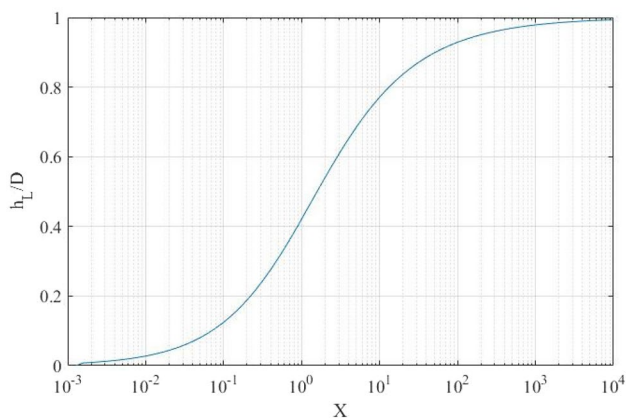


Fig. 8 The equilibrium level of liquid in the stratified regime

$$\tau_G = f_G \frac{\rho_G U_G^2}{2} \tag{3}$$

$$\tau_i = f_i \frac{\rho_G (U_G - U_L)^2}{2} \tag{4}$$

where liquid and gas velocities are defined by void fraction α :

$$U_L = \frac{U_{SL}}{1 - \alpha}, U_G = \frac{U_{SG}}{\alpha} \tag{5}$$

For a smooth tube, friction factors are defined as follows:

$$f_L = C_L \left(\frac{D_L U_L}{\nu_L} \right)^{-n}, D_L = \frac{4A_L}{S_L} \tag{6}$$

$$f_G = C_G \left(\frac{D_G U_G}{\nu_G} \right)^{-m}, D_G = \frac{4A_G}{S_G + S_i} \tag{7}$$

$C_L = C_G = 0.046, n = m = 0.2$ for a turbulent flow;
 $C_L = C_G = 16, n = m = 1$ for a laminar flow.

For a laminar flow in rectangular channels, constants C_L and C_G represent the aspect ratio function (Shah and London, 1978):

$$C_G = C_L = 24(1 - 1.3553AR + 1.9467AR^2 - 1.7012AR^3 + 0.9564AR^4 - 0.2537AR^5) \tag{8}$$

$$AR = b/h$$

Here τ_i, τ_g, τ_l are interface/gas/liquid shear stresses and S_i, S_g, S_l are interface, dry, and wetted perimeters, respectively. A_g, A_l are gas/liquid cross-section areas, ρ_g, ρ_l are gas/liquid densities, g is acceleration of gravity, β is the angle of inclination, f is the friction factor. The solution to Eq. 1 is shown in Fig. 5 via Martinelli parameter defined as follows:

$$X^2 = \frac{\frac{4C_L}{D} \left(\frac{U_{SL} D}{\nu_L} \right)^{-n} \frac{\rho_L U_{SL}^2}{2}}{\frac{4C_G}{D} \left(\frac{U_{SG} D}{\nu_L} \right)^{-m} \frac{\rho_G U_{SG}^2}{2}} = \frac{\left(\frac{dP}{dx} \right)_{SL}}{\left(\frac{dP}{dx} \right)_{SG}} \tag{9}$$

At the next step, it is checked whether the regime is the bubble one. The regime is the bubble one when $U_{SL} > U_{SG} \frac{1-\epsilon}{\epsilon}$, where gas content $\epsilon = 0.52$ and characteristic bubble diameter $d_C < d_{CD}$ are found from Eqs. 11 and 12; $d_C < d_{CB}$ is found from Eqs. 11 and 13. If the regime is not the bubble one, then it is checked whether it is stratified.

$$d_C = (0.725 + 4.15\epsilon^{0.5}) \left(\frac{\sigma}{\rho_L} \right)^{0.6} \kappa^{-0.4}, \kappa = \frac{2f_m}{D} U_m^3, U_m = U_{SL} + U_{SG} \tag{10}$$

$$d_{CD} = 2 \left[\frac{0.4\sigma}{(\rho_L - \rho_G)g} \right]^{0.5} \tag{11}$$

$$d_{CB} = \frac{3}{8} \frac{\rho_L}{\rho_L - \rho_G} \frac{f_M U_M^2}{g \cos \beta} \tag{12}$$

where κ is energy dissipation per unit mass.

The stratified regime is observed when it is stable from the point of view of the Kelvin–Helmholtz analysis when inequality 8 is satisfied and inequality 9 is not satisfied. If the regime is not the bubble and not the stratified, a check whether the regime is annular is required. For horizontal tubes, this is the condition when $X < 1.6$ (Taitel and Dukler 1976). If the regime is not the bubble, not the stratified, and not the annular, then it is intermittent. Two types of the intermittent regime were distinguished: the churn and the slug ones. The slug regime is observed when $\alpha_s > 0.52$ in Eq. 16.

$$F^2 \left[\frac{1}{C^2} \frac{(U_G/U_{SG})^2 D \cdot (dA_L/dh_l)}{A_G} \right] < 1 \tag{13}$$

$$F = \sqrt{\frac{\rho_G}{\rho_L - \rho_G} \frac{U_{SG}}{\sqrt{D} \cdot g \cos \beta}} \tag{14}$$

$$U_{SL}^2 > \frac{gd(1 - h_L/d) \cos \beta}{f_L} \tag{15}$$

$$s = 0.058 \left[d_c \left(\frac{2f_M}{D} U_M^2 \right)^{2/5} \left(\frac{\rho_L}{\sigma} \right)^{3/5} - 0.725 \right]^2 \tag{16}$$

The experimental study of a two-phase flow in a tube of a 5.1-cm diameter performed by Shoham (1982) is compared with the calculation by the Taitel (1990) model in Fig. 9. Good qualitative and quantitative agreement is observed; the data agree with an accuracy of more than 94%.

Experimental data obtained for the channels with cross-sections of $1 \times 29 \text{ mm}^2$, $0.05 \times 10 \text{ mm}^2$, $0.05 \times 20 \text{ mm}^2$, and $0.05 \times 10 \text{ mm}^2$, are compared in Fig. 10, where hydraulic diameter D_h is equivalent to the diameter of the round channels. In the above microchannels, the slug regime was not observed, but instead, the bubble regime was observed. This is since in wide minichannels (aspect ratio greater than 10)

in the bubble flow, the characteristic bubble sizes are almost always greater than the channel height, but much less than its width. In channels with a small aspect ratio (about 1), the bubble size in the bubble regime is always less than the channel height. Thus, the slug regime in round tubes corresponds to the bubble regime in slit microchannels, since in slit microchannels, the characteristic longitudinal and transverse dimensions of the bubble are greater than the channel height but less than its width.

Thus, according to the Taitel and Dukler model, the slug regime in wide channels can be the bubble regime in experiments. It can be seen in Fig. 10a that qualitatively the region of the slug regime, according to the Taitel and Dukler model, corresponds to the region of the bubble regime in the experiment with a microchannel of the $1 \times 29 \text{ mm}^2$ cross-section. The accuracy of bubble regime prediction by the Taitel and Dukler model was over 37%. The qualitative and quantitative prediction of the churn regime by the model also satisfactorily corresponds to the experimental data; the accuracy is more than 49%. In the experimental work, the jet regime, when the lower wall of the channel is not wetted and liquid moves along the sides of the channel, was also distinguished. This regime is a feature of wide minichannels and microchannels. It can also be seen that the model predicts rather

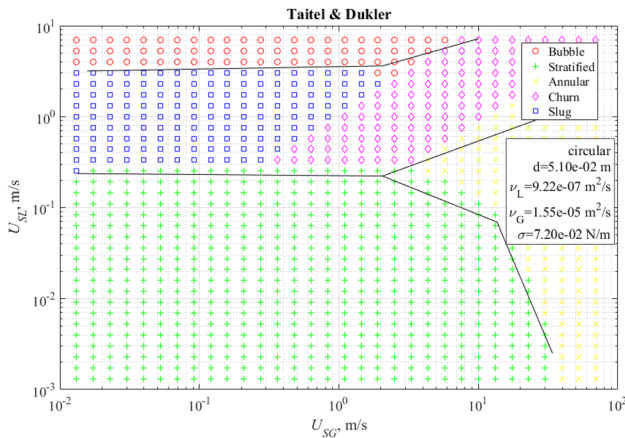


Fig. 9 Comparison of experimental data of Shoham (1982) (solid lines) with Taitel model (1990)

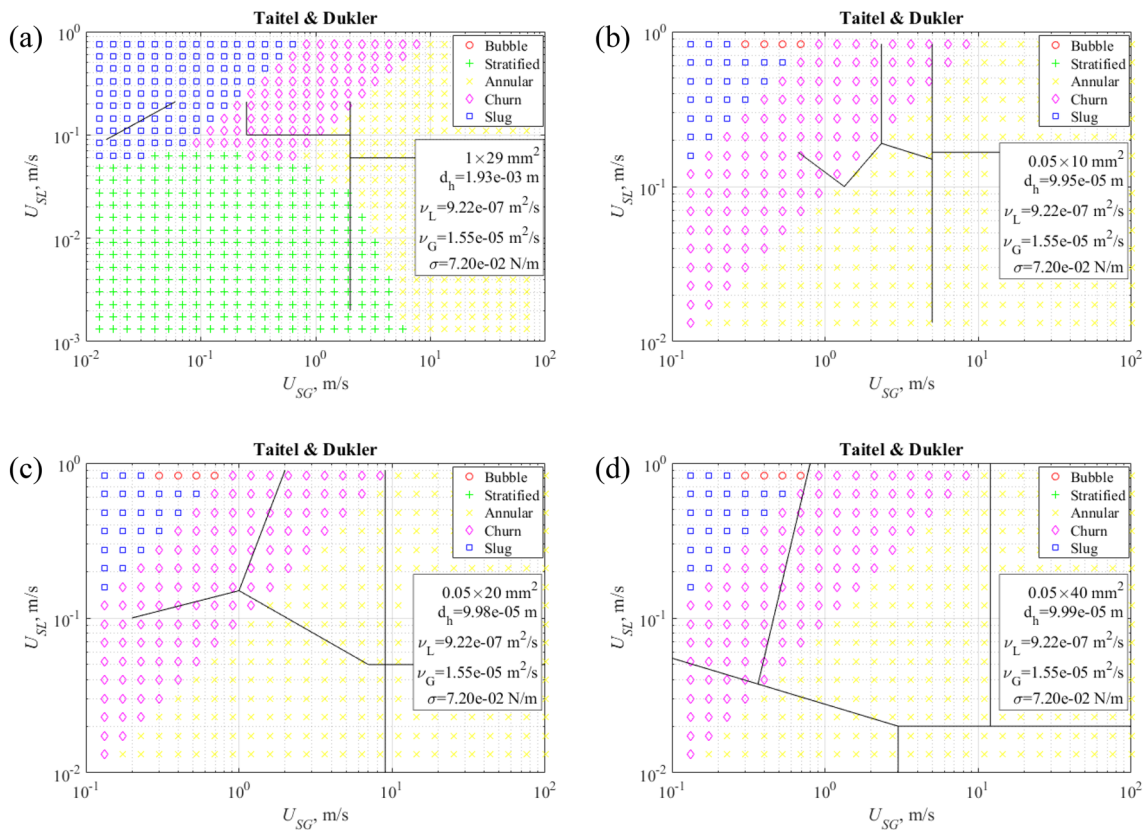


Fig. 10 Comparison of experimental data (solid lines) with the Taitel and Dukler model. Channel cross-section: a $1 \times 29 \text{ mm}^2$; b $0.05 \times 10 \text{ mm}^2$; c $0.05 \times 20 \text{ mm}^2$; d $0.05 \times 40 \text{ mm}^2$

poorly the boundary of transition from the stratified regime to the annular one.

The calculation by the Taitel and Dukler model for a channel with a cross-section of $0.05 \times 10 \text{ mm}^2$ is shown in Fig. 10b. It is seen that the model does not predict transitions between two-phase flow regimes for the specified channel. It should be noted that the microchannel width of the studied channel exceeds its height by more than two orders of magnitude. At that, changing the channel width has a negligible effect on the hydraulic diameter. It can be seen in Figs. 10b–d that when the channel width changes by a factor of 2 or even 4, the hydraulic diameter changes insignificantly; as a result, the difference between the calculated maps of Taitel and Dukler is not visible, whereas the differences between the experimental maps are significant.

The Taitel and Dukler model was also adapted for rectangular channels: in this case, the microchannel height and width were directly used for calculations. A comparison of the calculated regime maps of the original model and the model modified for rectangular channels is shown in Fig. 11. It can

be seen that for a channel with a cross-section of $1 \times 29 \text{ mm}^2$, the modified model predicts the transition to the churn flow better, while for microchannels with a height of $50 \text{ }\mu\text{m}$, there are almost no differences.

Thus, we can conclude that the Taitel and Dukler model has been developed for tubes; it predicts the boundaries of regimes in large channels well and does not describe experimental data in wide microchannels.

5 Comparison of experimental data with the Ullmann and Brauner model

An algorithm that calculates the boundaries between the regimes by the Ullmann and Brauner model (2007) has been developed. A comparison of the boundaries calculated by the Ullmann and Brauner (2007) model with the experimental data of Triplett et al. (1999) in a channel with diameter $D = 1.097 \text{ mm}$ is shown in Fig. 12. Boundary 1 is calculated using Eq. 11 where the value $(\epsilon_G)_{crit} = 0.15$ is used. Boundary

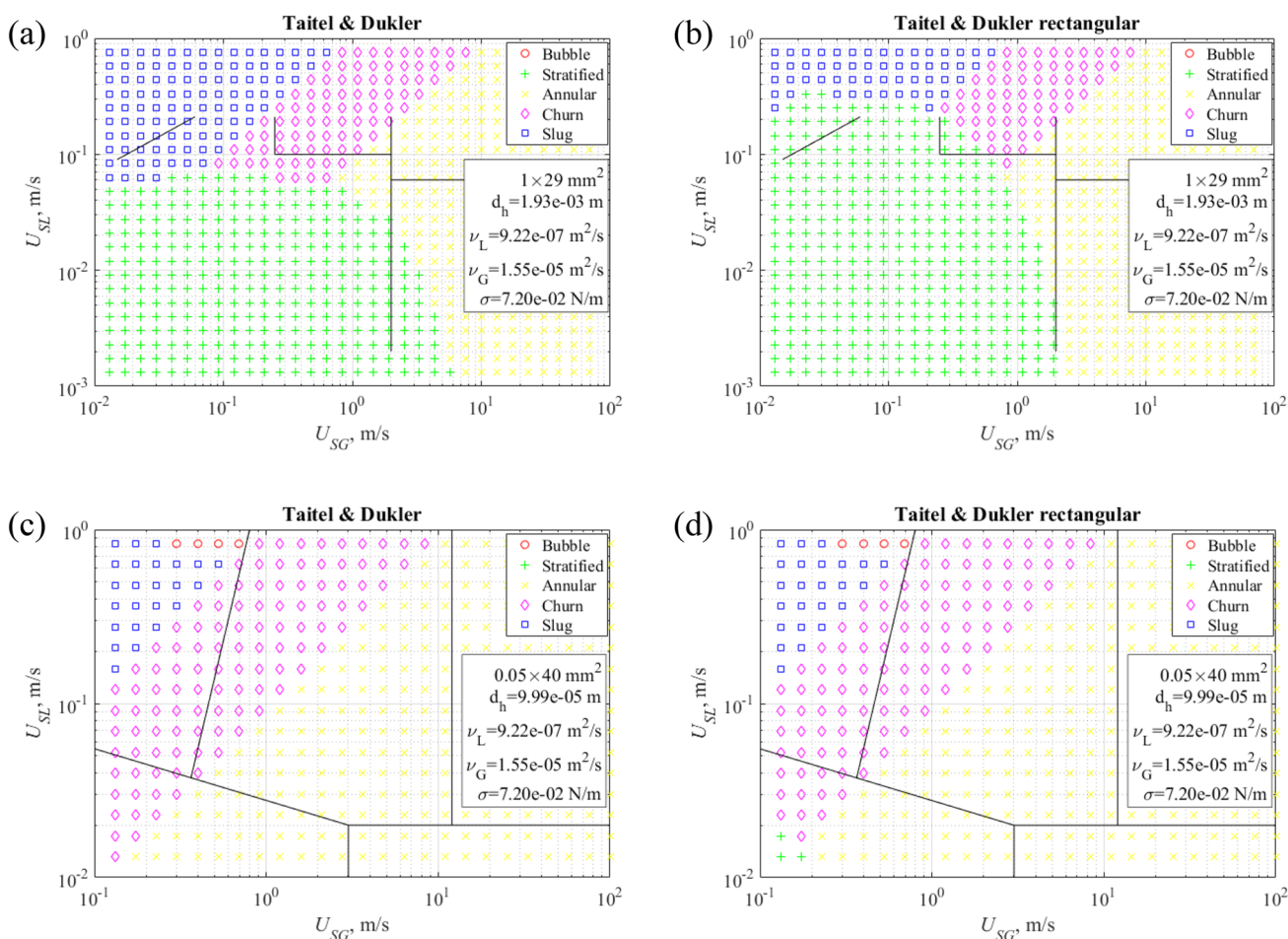


Fig. 11 Comparison of experimental data (solid lines) with the Taitel and Dukler model. Channel cross-section: **a** original model, $1 \times 29 \text{ mm}^2$; **b** model for a rectangular channel, $1 \times 29 \text{ mm}^2$; **c** original model, $0.05 \times 40 \text{ mm}^2$; **d** model for a rectangular channel, $0.05 \times 40 \text{ mm}^2$

2 was calculated from condition 12, where the following expressions for the bubble size were used:

$$U_{SL} = \frac{1 - (\epsilon_G)_{crit}}{(\epsilon_G)_{crit}} U_{SG} \tag{17}$$

$$d_{max} = \max\{(d_{max})_o, (d_{max})_\epsilon\} \leq d_{crit} = \min\{d_{L\sigma}, d_{Lb}, 0.5D\} \tag{18}$$

$$(\tilde{d}_{max})_o = \frac{d_{max}}{D} = 30We_L^{-1} Re_L^{0.2} \tag{19}$$

$$(\tilde{d}_{max})_\epsilon = \frac{d_{max}}{d} = 174C_K We_L^{-1} Re_L^{0.2} \frac{\epsilon_G}{1 - \epsilon_G} \tag{20}$$

In Eq. 14, the values of U_{SL} and U_{SG} are set implicitly; therefore, the Newton–Raphson method was used for the solution. Equation 15, including value $\epsilon_L^{crit} = 0.4$, was used to plot Boundary 3. Boundary 4 was calculated from Eq. 16. Equation 17 was used to calculate Boundary 5.

$$U_{SG} \geq \tilde{\epsilon} \left[\tilde{\epsilon} \frac{\mu_L}{\mu_G} + 2 \right] U_{SL}; \tilde{\epsilon} = \frac{1 - \epsilon_L^{crit}}{\epsilon_L^{crit}} \tag{21}$$

$$\Delta U_G = U_G - U_L \geq 4.9 \left[\frac{\sigma}{\rho_G D} \right]^{0.5} F(On); Re_G > 2100 \tag{22}$$

$$(U_M)_{crit} = (U_{SG} + U_{SL})_{crit} = 9,72 \left[\frac{\sigma}{\rho_L^{0.8} \mu_L^{0.2} D^{0.8}} \right]^{0.55} \tag{23}$$

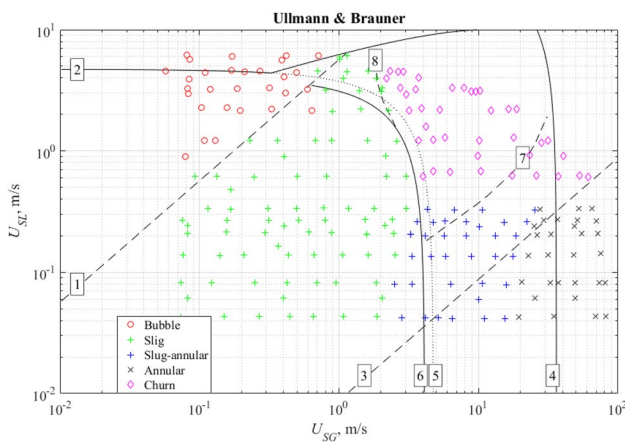


Fig. 12 Comparison of experimental data of Triplett et al. (1999) (markers in the figure) with the Ullmann and Brauner model (2007)

$$(U_M)_{crit} = (U_{SG} + U_{SL})_{crit} = 16 \left[\frac{\sigma}{\rho_L D} \right]^{0.5} \tag{24}$$

When plotting Boundary 6, Eq. 18 was applied. Boundaries 7 and 8 are taken from the Ullmann and Brauner model (2007) for the slug flow of Brauner and Ullmann (2004).

According to Fig. 12, the calculations by the Ullmann and Brauner model (2007) are in good agreement with the experimental data of Triplett et al. (1999) in a round channel with a diameter $D = 1.097$ mm. The accuracy of bubble regime prediction is higher than 93%. The slug regime is calculated by the model with the addition of Brauner and Ullmann (2004) with an accuracy of more than 92%. The boundary between the annular and slug regimes is calculated with an accuracy of more than 90%. It can be seen from the figure that the Ullmann and Brauner model (2007) predicts the transition from the annular to the churn regime worse; it can be seen that the boundaries in calculations and experimental data are qualitatively different, whereas the transition from the slug regime to the churn one is predicted by the model with the addition of Brauner and Ullmann (2004) with high accuracy (over 94%).

Calculations of regime maps by the Ullmann and Brauner model (2007) are compared with experimental results in Fig. 13. Figure 13a shows a comparison of data for a channel with a cross-section of 1×29 mm². Instead of the slug regime, according to the Ullmann and Brauner model (2007), the jet regime was observed, which is explained by the difference in the channel geometry. Very good qualitative and quantitative calculation accuracy of the transition from the jet regime to the bubble one is observed: more than 60%. The model also predicts the transition from the jet regime to the stratified and annular regimes with high accuracy: higher than 80% and 90%, respectively. However, the model does not predict transitions to the churn regime and from the stratified regime to the annular one.

According to Fig. 13b, for a channel with a cross-section of 0.05×10 mm², the Ullmann and Brauner model (2007) does not predict transitions between the regimes. Whereas for the channels with a height of 50 μ m and width of 20 and 40 mm, Fig. 13c, d, the Ullmann and Brauner model (2007) predicts very well the transition from the jet regime to the stratified one (in a channel of 0.05×20 mm² with an accuracy of more than 85%; and a channel of 0.05×40 mm² with an accuracy of about 60%) and from the churn regime to the annular one (in both channels, all experimental points coincide with calculations by the Ullmann and Brauner model (2007)).

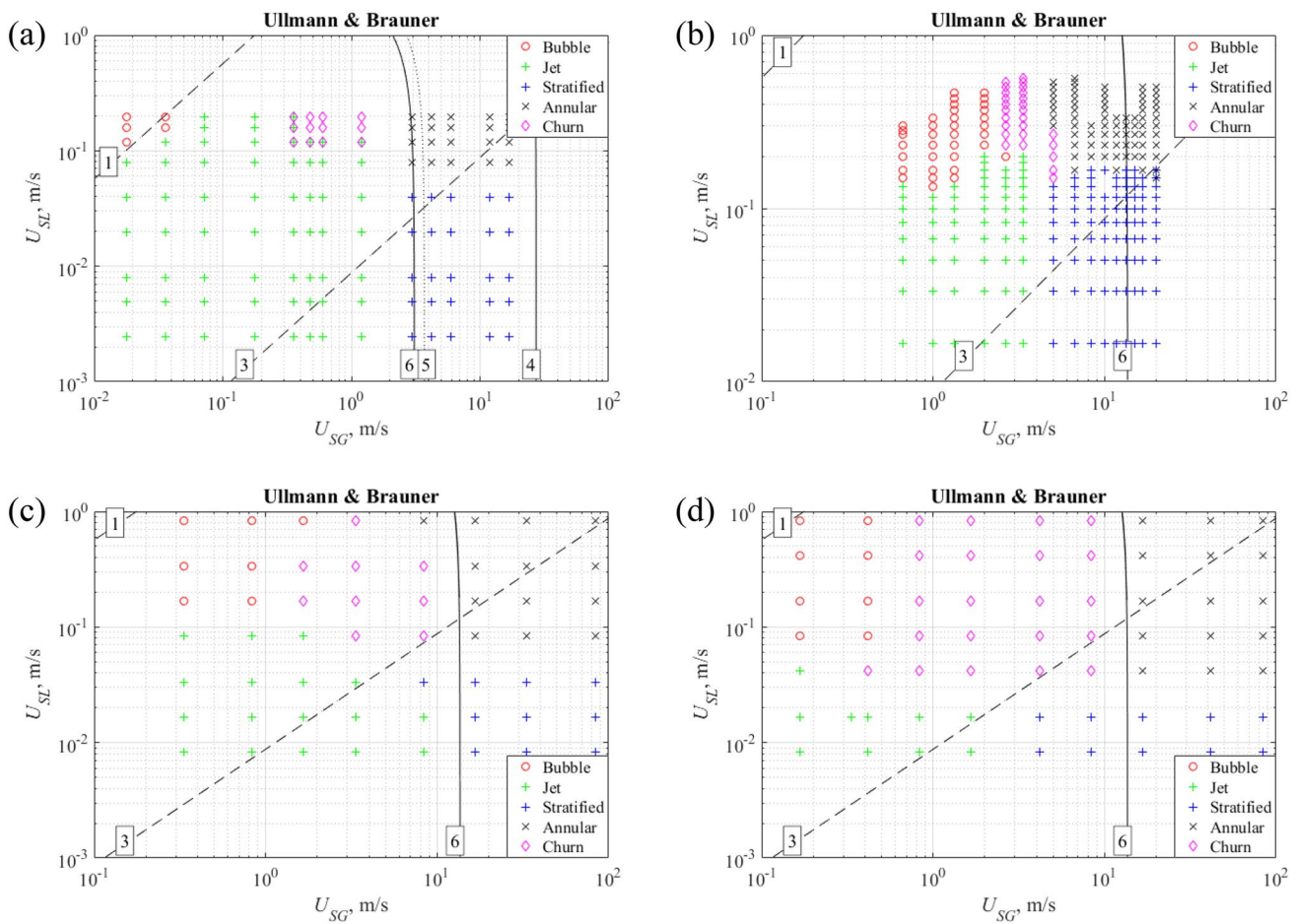


Fig. 13 Comparison of experimental data (solid lines) with the Ullmann and Brauner model (2007). Channel cross-section: **a** $1 \times 29 \text{ mm}^2$; **b** $0.05 \times 10 \text{ mm}^2$; **c** $0.05 \times 20 \text{ mm}^2$; **d** $0.05 \times 40 \text{ mm}^2$

6 Transition to the annular regime

In the considered models, the transition from the stratified to the annular regime is determined by the channel diameter. However, as it was found experimentally, this transition depends only on the width of a flat microchannel. This occurs because of the film formation on the upper wall of the channel caused by the pulsation of jets moving in the central part of the microchannel, Fig. 14. The number of jets N is proportional to the microchannel width b . In this case, the transition to the annular regime depends on the liquid velocity, when it is sufficient for the formation of a film, and on the microchannel width. Moreover, the wider the microchannel, the more liquid jets are formed and the transition to the annular regime occurs at a lower liquid velocity. Thus, it is possible to introduce the critical dimensionless numbers We_{an} and Re_{an} for the transition to the annular regime:

$$Re_{an} = \frac{bU_{SL}}{\nu_L}; We_{an} = \frac{\rho_L b U_{SL}^2}{\sigma} \tag{25}$$

Then the transition from the stratified flow to the annular one is determined by the following equation, derived

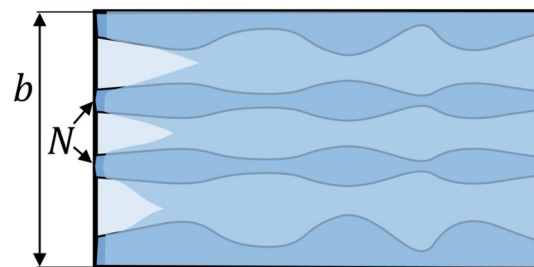


Fig. 14 Formation of the annular flow

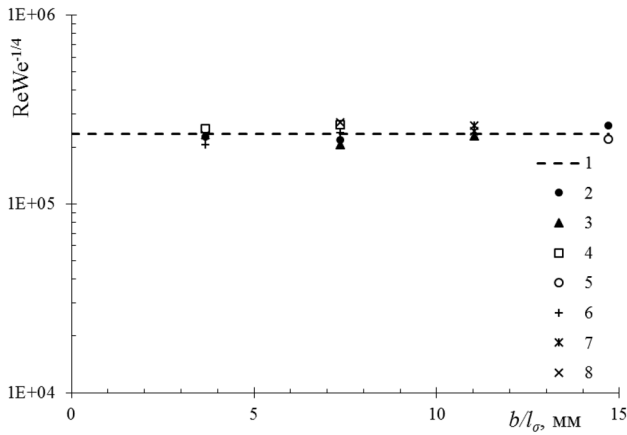


Fig. 15 Dependence of criterion $Re_{an} We_{an}^{-1/4} = 2.3 \cdot 10^5$ on dimensionless parameter b/l_{σ} for the developed model (1) and experimental data for the channels with the height of (2) 50 μm ; (3) 100 μm ; (4) 150 μm ; (5) 200 μm ; (6) 300 μm ; (7) 440 μm ; (8) 1000 μm

empirically for the channels with a height of 0.05–1 mm and a width of 10–40 mm:

$$Re_{an} We_{an}^{-1/4} = 2.3 \cdot 10^5 \tag{26}$$

The dependence of criterion $Re_{an} We_{an}^{-1/4} = 2.3 \cdot 10^5$ on dimensionless parameter b/l_{σ} for the developed model and experimental results for the minichannels and microchannels with a height of 0.05–1 mm and width of 10–40 mm is presented in Fig. 15. It can be seen in the diagram that all transition boundaries for the given channels are in good agreements with the developed model.

The developed model of transition to the annular regime (Eq. 20, shown in the figure by dashed line 1) and transition to the annular regime by the Ullmann and Brauner model (2007) (Eq. 18, shown in the figure by solid line 2) are compared in Fig. 16. It can be seen that both models determine the transition to the annular regime with good accuracy.

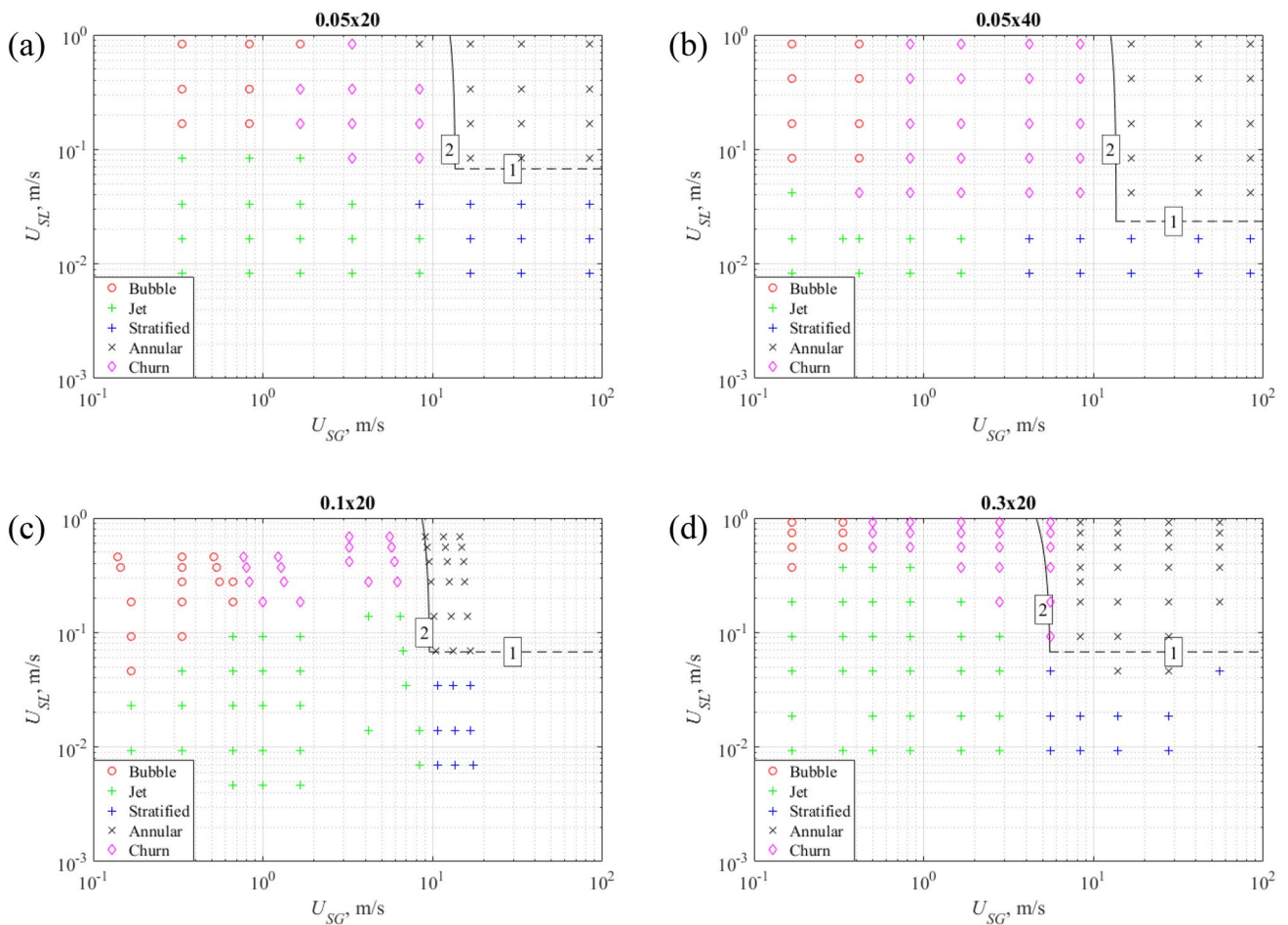


Fig. 16 Comparison of experimental data (markers) with the Ullmann and Brauner model. Channel cross-section: **a** 0.05 \times 20 mm²; **b** 0.05 \times 40 mm²; **c** 0.1 \times 20 mm²; **d** 0.3 \times 20 mm²

7 Conclusion

A two-phase flow in flat minichannels and microchannels with a height range of 50 μm –1 mm and a width range of 10–40 mm is experimentally investigated in this work. The flow regimes have been determined. For the quantitative analysis of the transitions between the flow regimes, two different approaches were used: the LIF technique and the Schlieren one with automated image post-processing. The Schlieren technique allows one to characterize the liquid distribution over the channel cross-sections and to measure the thin liquid films. Nevertheless, with a decrease in the channel height, the resolution of this technique is insufficient for characterizing thin liquid films. In this regard, for a channel height of less than 300 μm , the Schlieren technique was applied. The automated post-processing algorithm that calculates local void fraction, bubble size, bubble formation frequency, and liquid film areas was developed to analyze Schlieren images. Using these quantitative characteristics, the maps of two-phase flow regimes were created for the wide range of channel cross-sections. Comparison of experimental regimes of the two-phase flow in wide microchannels with theoretical models demonstrates that the proposed models describe well only a narrow range of channels (mainly round channels). In wide microchannels, the picture is significantly different. In addition, the models do not take into account many factors (for example, wettability of the channel surface), which begin to play an important role with a decrease in the size of microchannels. Despite this, it is worth noting that the Ullmann and Brauner model (2007) predicts quite well the transition to the stratified and the annular flow regimes in channels with cross-sections of $0.05 \times 20 \text{ mm}^2$ and $0.05 \times 40 \text{ mm}^2$. Regularities of the channel width influence on the transition to the annular regime have been revealed. A criterion for the transition from the stratified to the annular regime, based on the discovered fact of liquid jet structuring along the channel, is proposed.

Author contributions FR: conceptualization, methodology, software, investigation, writing—original draft, writing—review and editing. YD: formal analysis, writing—review and editing. EC: conceptualization, methodology, writing—original draft, writing—review and editing, supervision.

Funding This work was financially supported by the Russian Science Foundation (grant no. 22-19-20090), <https://rscf.ru/project/22-19-20090/> and the Government of the Novosibirsk Region, Agreement no. P-13.

Availability of data and materials Any datasets used can be requested from corresponding author.

Declarations

Conflict of interest The authors have declared that there is no conflict of interest.

Ethical approval Not applicable.

References

- Baker O (1954) Simultaneous Flow of Oil and Gas. *Oil Gas J* 53(12):185–195
- Bar-Cohen A, Rahim E (2009) Modeling and prediction of two-phase microgap channel heat transfer characteristics. *Heat Transf Eng* 30(8):601–625. <https://doi.org/10.1080/01457630802656678>
- Barnea D, Shoham O, Taitel Y, Dukler AE (1980) Flow pattern transition for gas-liquid flow in horizontal and inclined pipes. Comparison of experimental data with theory. *Int J Multiph Flow* 6:217–226. [https://doi.org/10.1016/0301-9322\(80\)90012-9](https://doi.org/10.1016/0301-9322(80)90012-9)
- Bar-Cohen A, Sheehan J R, Rahim E (2012) Two-phase thermal transport in microgap channels—theory, experimental results, and predictive relations. *Microgravity Science and Technology* 24:1–15. <https://doi.org/10.1007/s12217-011-9284-3>
- Brauner N, Ullmann A (2004) Modelling of gas entrainment from Taylor bubbles. Part A: Slug flow. *Int J Multiph Flow* 30:273–290. <https://doi.org/10.1016/j.ijmultiphaseflow.2003.11.007>
- Chinnov EA, Ronshin FV, Kabov OA (2015) Study of gas-water flow in horizontal rectangular channels. *Thermophys Aeromechanics* 22(5):621–629. <https://doi.org/10.1134/S0869864315050108>
- Chinnov EA, Ronshin FV, Kabov OA (2016) Two-phase flow patterns in short horizontal rectangular microchannels. *Int J Multiph Flow* 80:57–68. <https://doi.org/10.1016/j.ijmultiphaseflow.2015.11.006>
- Choi C W, Yu D I, Kim M H (2010) Adiabatic two phase flow in rectangular microchannels with different aspect ratios: Part II—bubble behaviors and pressure drop in single bubble. *International Journal of Heat and Mass Transfer* 53(23–24):5242–5249. <https://doi.org/10.1016/j.ijheatmasstransfer.2010.07.035>
- Chung P Y, Kawaji M (2004) The effect of channel diameter on adiabatic two-phase flow characteristics in microchannels. *International journal of multiphase flow* 30(7–8):735–761. <https://doi.org/10.1016/j.ijmultiphaseflow.2004.05.002>
- Der O, Bertola V (2020) An experimental investigation of oil-water flow in a serpentine channel. *Int J Multiph Flow*. <https://doi.org/10.1016/j.ijmultiphaseflow.2020.103327>
- Drummond KP, Weibel JA, Garimella SV (2020) Two-phase flow morphology and local wall temperatures in high-aspect-ratio manifold microchannels. *Int J Heat Mass Transf* 153:119551. <https://doi.org/10.1016/j.ijheatmasstransfer.2020.119551>
- Iqbal A, Pandey M (2018) Effect of local thermophysical properties and flashing on flow boiling pressure drop in microchannels. *Int J Multiph Flow* 106:311–324. <https://doi.org/10.1016/j.ijmultiphaseflow.2018.05.020>
- Kawahara A., Chung PY, Kawaji M (2002) Investigation of two-phase flow pattern, void fraction and pressure drop in a microchannel. *International journal of multiphase flow* 28(9):1411–1435. [https://doi.org/10.1016/S0301-9322\(02\)00037-X](https://doi.org/10.1016/S0301-9322(02)00037-X)
- Li X, Huang Y, Wu Z, Gu H, Chen X (2021) High conversion hydrogen peroxide microchannel reactors: Design and two-phase flow instability investigation. *Chem Eng J* 422:130080. <https://doi.org/10.1016/j.cej.2021.130080>
- Li Q, Guo W, Li H, Peng Z, Liu J, Chen S, Wang G (2022) Experimental study of Taylor bubble flow in non-Newtonian liquid in a

- rectangular microchannel. *Chem Eng Sci* 252:117509. <https://doi.org/10.1016/j.ces.2022.117509>
- Magnini M, Thome JR (2017) An updated three-zone heat transfer model for slug flow boiling in microchannels. *Int J Multiph Flow* 91:296–314. <https://doi.org/10.1016/j.ijmultiphaseflow.2017.01.015>
- Mandhane JM, Gregory GA, Aziz K (1974) A flow pattern map for gas-liquid flow in horizontal pipes. *Int J Multiph Flow* 1:537–553. [https://doi.org/10.1016/0301-9322\(74\)90006-8](https://doi.org/10.1016/0301-9322(74)90006-8)
- Moriyama K, Inoue A, Ohira H (1993) The thermohydraulic characteristics of two-phase flow in extremely narrow channels (the frictional pressure drop and heat transfer boiling two-phase flow, analytical model). *Heat Transf Res;(United States)* 21(8)
- Nasr MH, Green CE, Kottke PA, Zhang X, Sarvey TE, Joshi YK, Bakir MS, Fedorov AG (2017) Hotspot thermal management with flow boiling of refrigerant in ultrasmall microgaps. *J Electron Packag Trans ASME* 139:011006–011011. <https://doi.org/10.1115/1.4035387>
- Oudah SK, Fang R, Tikadar A, Salman AS, Khan JA (2020) An experimental investigation of the effect of multiple inlet restrictors on the heat transfer and pressure drop in a flow boiling microchannel heat sink. *Int J Heat Mass Transf* 153:119582. <https://doi.org/10.1016/j.ijheatmasstransfer.2020.119582>
- Ronshin FV, Cheverda VV, Chinnov EA, Kabov OA (2016) Features of two-phase flow regimes in a horizontal rectangular microchannel with the height of 50 μm . *Interfacial Phenomena Heat Transf* 4(2–3):191–205. <https://doi.org/10.1615/InterfacPhenomHeatTransf.2017020238>
- Ronshin F, Chinnov E (2019) Experimental characterization of two-phase flow patterns in a slit microchannel. *Exp Therm Fluid Sci* 103:262–273. <https://doi.org/10.1016/j.expthermflusci.2019.01.022>
- Ronshin FV, Dementyev YA, Chinnov EA, Cheverda VV, Kabov OA (2019) Experimental investigation of adiabatic gas-liquid flow regimes and pressure drop in slit microchannel. *Microgravity Sci Technol* 31(5):693–707. <https://doi.org/10.1007/s12217-019-09747-1>
- Saisorn S, Wongwises S (2009) An experimental investigation of two-phase air–water flow through a horizontal circular micro-channel. *Experimental Thermal and Fluid Science* 33(2):306–315. <https://doi.org/10.1016/j.expthermflusci.2008.09.009>
- Serizawa A, Feng Z, Kawara Z (2002) Two-phase flow in microchannels. *Experimental Thermal and Fluid Science* 26(6–7):703–714. [https://doi.org/10.1016/S0894-1777\(02\)00175-9](https://doi.org/10.1016/S0894-1777(02)00175-9)
- Shoham O (1982) Flow pattern transition and characterization in gas-liquid flow in inclined pipes. PhD. Dissertation, Tel-Aviv University, Ramat-Aviv, Israel
- Soma S, Kunugi T (2020) Phenomenological model for non-isothermal capillary evaporation in narrow channel. *Int J Multiph Flow* 122:103154. <https://doi.org/10.1016/j.ijmultiphaseflow.2019.103154>
- Sur A, Liu D (2012) Adiabatic air–water two-phase flow in circular microchannels. *International Journal of Thermal Sciences* 53:18–34. <https://doi.org/10.1016/j.ijthermalsci.2011.09.021>
- Taitel Y (1990) Flow pattern transition in two phase flow. In: Ch M (ed) *International Heat Transfer Conference Digital Library*. Begel House Inc. <https://doi.org/10.1615/IHTC9.1930>
- Taitel Y, Barnea D (2016) Modeling of gas liquid flow in pipes. In: Thome J (ed) *Encyclopedia of two-phase heat transfer and flow. I. Fundamentals and methods*, 1st edn. World Scientific Publishers, New Jersey
- Taitel Y, Dukler AE (1976) A model for predicting flow regime transitions in horizontal and near horizontal gas-liquid flow. *AIChE J* 22:47–55. <https://doi.org/10.1002/aic.690220105>
- Taitel Y, Dukler AE (1987) Effect of pipe length on the transition boundaries for high-viscosity liquids. *Int J Multiph Flow* 13:577–581. [https://doi.org/10.1016/0301-9322\(87\)90023-1](https://doi.org/10.1016/0301-9322(87)90023-1)
- Triplett KA, Ghiaasiaan SM, Abdel-Khalik SI, Sadowski DL (1999) Gas-liquid two-phase flow in microchannels part I: two-phase flow patterns. *Int J Multiph Flow* 25(3):377–394. [https://doi.org/10.1016/S0301-9322\(98\)00054-8](https://doi.org/10.1016/S0301-9322(98)00054-8)
- Ullmann A, Brauner N (2007) The prediction of flow pattern maps in minichannels. *Multiph Sci Technol*. <https://doi.org/10.1615/MultScienTechn.v19.i1.20>
- Weisman J, Duncan D, Gibson J, Crawford T (1979) Effects of fluid properties and pipe diameter on two-phase flow patterns in horizontal lines. *Int J Multiph Flow* 5:437–462. [https://doi.org/10.1016/0301-9322\(79\)90031-4](https://doi.org/10.1016/0301-9322(79)90031-4)
- Wu B, Firouzi M, Mitchell T, Rufford TE, Leonardi C, Towler B (2017) A critical review of flow maps for gas-liquid flows in vertical pipes and annuli. *Chem Eng J* 326:350–377. <https://doi.org/10.1016/j.cej.2017.05.135>
- Xiong T, Liu G, Huang S, Yan G, Yu J (2022) Two-phase flow distribution in parallel flow mini/micro-channel heat exchangers for refrigeration and heat pump systems: a comprehensive review. *Appl Thermal Eng* 201:117820. <https://doi.org/10.1016/j.applthermaleng.2021.117820>
- Yao C, Zhao Y, Ma H, Liu Y, Zhao Q, Chen G (2021) Two-phase flow and mass transfer in microchannels: A review from local mechanism to global models. *Chem Eng Sc* 229:116017. <https://doi.org/10.1016/j.ces.2020.116017>
- Yin Y, Zhu C, Guo R, Fu T, Ma Y (2018) Gas-liquid two-phase flow in a square microchannel with chemical mass transfer: Flow pattern, void fraction and frictional pressure drop. *Int J Heat Mass Transf* 127:484–496. <https://doi.org/10.1016/j.ijheatmasstransfer.2018.07.113>
- Zaitsev D, Tkachenko E, Kabov O (2017) An experimental study of high heat flux removal by shear-driven liquid films. *EPJ Web Conf* 159:00054. <https://doi.org/10.1051/epjconf/201715900054>

Publisher's Note Springer Nature remains neutral with regard to jurisdictional claims in published maps and institutional affiliations.

Springer Nature or its licensor (e.g. a society or other partner) holds exclusive rights to this article under a publishing agreement with the author(s) or other rightsholder(s); author self-archiving of the accepted manuscript version of this article is solely governed by the terms of such publishing agreement and applicable law.